

Optimization of reconstruction parameters in [¹⁸F]FDG PET brain images aiming scan time reduction

Otimização de parâmetros de reconstrução de imagens PET cerebrais adquiridas com [¹⁸F]FDG visando a redução do tempo de exame

Samara Pinto¹, Paulo R. R. V. Caribe^{1,2}, Lucas Narciso^{1,3}, Ana Maria Marques da Silva¹

¹Medical Image Computing Laboratory (MEDICOM), PUCRS, Porto Alegre, Brazil

²Medical Imaging and Signal Processing (MEDISIP), Ghent University, Ghent, Belgium

³Department of Medical Biophysics, Western University, London, Canada

Abstract

Iterative image reconstruction methods are widely used in PET due to their better image quality when compared to analytical methods. However, inaccurate quantification occurs in low activity concentration regions, which leads to biased quantification of PET images. The diagnosis of some neurodegenerative diseases, such as Alzheimer's disease, is based on identifying such low-uptake regions. Furthermore, PET imaging in these populations should be as short as possible to limit head movements and improve patient comfort. This work aims to identify optimized reconstruction parameters of [¹⁸F]FDG PET brain images aiming to reduce image acquisition time with minimal impact on quantification. For this, [¹⁸F]FDG PET images of a Hoffman 3-D brain phantom were acquired. Analytical and iterative reconstruction methods were compared utilizing image quality and quantitative accuracy metrics. OSEM reconstruction algorithm was optimized (4 iterations and 32 subsets). It resulted in remarkably similar images compared to the current clinical settings, with a 50% reduction in scan time (5 min with a post-reconstruction filter of 4 mm). Future clinical studies are needed to confirm the results presented here.

Keywords: brain PET; reconstruction; optimization; quantification; image quality; Hoffman

Resumo

Os métodos de reconstrução de imagens PET mais empregados são os iterativos, pois proporcionam uma imagem de melhor qualidade comparada com os métodos analíticos. No entanto, uma quantificação inadequada ocorre em regiões de baixa concentração de atividade, que levam a erros de quantificação das imagens PET. O diagnóstico de algumas doenças neurodegenerativas, como a doença de Alzheimer, é baseado na identificação de regiões de baixa captação. Além disso, o exame de PET para essas populações devem ser o mais curto possível, para limitar movimentos e melhorar o conforto do paciente. Este trabalho tem como objetivo identificar parâmetros de reconstrução otimizados de imagens cerebrais PET com [¹⁸F]FDG visando reduzir o tempo de aquisição com mínimo impacto na quantificação. Para tanto, foram adquiridas imagens PET do fantoma cerebral 3-D Hoffman, com [¹⁸F]FDG. Métodos de reconstrução analíticos e iterativos foram comparados para analisar a qualidade da imagem e as métricas de exatidão quantitativa. O algoritmo de reconstrução OSEM foi otimizado (4 iterações e 32 subsets) e resultou em imagens notavelmente similares àquelas obtidas com o padrão clínico atual, para uma redução de 50% no tempo de exame (5 min, com um filtro de pós-reconstrução de 4 mm). Estudos clínicos futuros são necessários para confirmar os resultados apresentados aqui.

Palavras-chave: PET cerebral; reconstrução; otimização; quantificação; qualidade de imagem; Hoffman

1. Introduction

Nuclear medicine is a medical imaging modality, often non-invasive, that provides metabolic and functional information *in vivo* in the format of dynamic or static images, representing the volumetric distribution of radiopharmaceuticals (1). Positron emission tomography (PET) is an imaging modality within nuclear medicine that uses positron emitter radiotracers and has excellent applicability in oncology, cardiology and neurology (2).

For decades, PET brain imaging has been widely used to study brain disorders, such as neurodegenerative diseases, dementia, epilepsy, neurodevelopmental and psychic disorders (3–5). Diagnosis of brain disorders with PET is accomplished by using specific radiotracers and analyzing brain activity (6). One of the most commonly used radiotracers, fluorodeoxyglucose labelled with ¹⁸F ([¹⁸F]FDG), can provide early signs of neuronal changes (7). FDG is an irreversibly bound tracer that provides direct or indirect measurements of glucose consumption, thus energy production, such as the

cerebral metabolic rate of glucose (8). Several studies have reported the possibility of using low activity injection for different PET radiotracers (9–14).

An increase in dementia cases in the elderly population is expected, which brings the need for better ways to detect and prevent symptoms earlier. In ageing, cognitive decline is typical, and it is usually aggravated by some neurodegenerative disease, such as Alzheimer's Disease (AD) (15). AD is characterized by progressive impairment, affecting cognition, memory and executive functions (15). In AD, low-uptake regions in [¹⁸F]FDG PET brain images are due to glucose metabolism impairment caused by neuronal loss (6). Thus, to assist in AD diagnosis, physicians use an uptake quantification tool and look for regions that present a reduced metabolic rate of glucose (low-uptake regions) (4).

PET image quantification of low-uptake regions is challenging, mainly due to low signal-to-noise ratio (SNR) and partial volume effects that affect the detectability of small lesions (4,9,16). However, the reliability of quantification can be improved during

image reconstruction by using iterative reconstruction techniques (1,17,18). The most widely used iterative reconstruction algorithm is the ordered subset expectation maximization (OSEM). An advantage of this algorithm is the ability to better model the emission and detection process. The effects of attenuation, detector normalization, and contamination by scattering and randoms are corrected in the reconstruction algorithm (19). In specific for the AD population, a reduction in scan time is essential to limit head movements, impacting quantification and increasing patient comfort (19,20).

This work aims to identify optimized reconstruction parameters of [¹⁸F]FDG PET brain images aiming to reduce image acquisition time with minimal impact on quantification. For this, [¹⁸F]FDG PET images were acquired of a Hoffman 3-D brain phantom, and image quality parameters and quantitative accuracy were evaluated for different reconstruction settings.

2. Materials and Methods

Data were acquired in a PET/computed tomography (CT) scanner (General Electric Medical System, Discovery 600; bismuth germanium oxide detector crystals) at the Brain Institute (Brains), Porto Alegre, Brazil. This study was conducted by acquiring images from the Hoffman 3-D brain phantom.

[¹⁸F]FDG-PET images were acquired in a Hoffman 3-D anthropomorphic brain simulator (Figure 1). This phantom consists of 40 acrylic slices (variable thickness, maximum of 3.0 mm) with a shape that simulates the regions of activity distribution. The different thicknesses produce a grey-to-white matter ratio (contrast) of 4:1.



Figure 1. Hoffman 3-D brain phantom consists of a cylinder with 40 independent cross-sections. Source: BIODIX (2021).

PET data were acquired in list-mode (10 min) after the injection of 37 MBq of [¹⁸F]FDG (25.6 kBq/ml). For comparison, the [¹⁸F]FDG activity usually injected in the clinic ranges from 5 to 20 mCi (185 to 740 MBq) (21), and approximately 8% of the injected activity is absorbed by the brain (22). Thus, the resulting brain activity concentration ranges from 10 to 42 kBq/mL (considering an average brain weight and density of 1.3 kg (23) and 1.08 g/mL (24), respectively).

Images were obtained with the standard reconstruction algorithm for comparison: OSEM (300-

mm FOV, 8 iterations, 16 subsets, 3.0-mm full-width half-maximum (FWHM) post-reconstruction smoothing filter, 192×192 voxels image matrix, 16-bits per pixel, 0.640 pixels/mm resolution, 1.56×1.56 mm² pixel size, and 47 axial slices of 3.27 mm thickness), as recommended by the manufacturer and used as the clinical settings for brain images at Brains. The OSEM iterative reconstruction method is commercially known as Vue-Point HD® and consists of implementing the 3D-maximum likelihood-OSEM algorithm with all the corrections incorporated during the iterative process (25).

Attenuation correction was applied using a CT-based map acquired before PET. Further corrections required for quantification (detector normalization, data rebinning, decay, dead-time, scatter, and random incidences) were also applied. Static PET images are presented in a single frame and represent the average radioactive concentration for a given time interval. In this study, static PET images were generated using 10 min, 5 min, 2.5 min, and 1 min post-acquisition start.

2.1. Quantitative accuracy

Quantification accuracy was evaluated by measurements of recovery coefficient (RC), grey-to-white matter activity concentration ratio (contrast) and bias. The measurements were obtained by automatically generating volumes-of-interest (VOIs) in the structural image (CT) and transferring them to the static PET images.

The measured-to-true activity concentration ratio (Eq. (1)), also known as recovery coefficient (RC), represents the fraction of the true activity concentration (C_{true}) present in the final image. C_{true} (= 25.6 kBq/ml) was calculated as the injected activity divided by the volume of water in the phantom after correcting for decay and residual activity in the syringe.

$$RC = \frac{C_{VOI}}{C_{true}} \tag{1}$$

where C_{VOI} is the measured activity concentration (in Bq/mL) in a VOI. Moreover, the contrast was calculated using Eq. (2). In this study, white matter (WM) was used as the background region.

$$Contrast = \frac{C_{GM}}{C_{WM}} \tag{2}$$

Quantification bias describes the difference between measured (C_{meas}) and expected (C_{exp}) activity concentrations. In this work, the percentage difference relative to the expected activity concentration at full statistics count-level (10 min) is used to estimate bias (13), as given by Eq. (3).

$$Bias (\%) = 100 \frac{C_{meas} - C_{exp}}{C_{exp}} \tag{3}$$

2.2. Image Quality

In addition to quantification accuracy, image quality was assessed utilizing noise, coefficient of variation (COV), SNR, and contrast-to-noise ratio (CNR). These measurements were also obtained by automatically generating VOIs in the CT image and transferring them to the static PET images.

Data variability can be measured by the COV, which is calculated as the ratio between the standard deviation (STD) and the mean activity concentration in the grey matter (GM). Finally, SNR and CNR are given by Eqs. (4) and (5), respectively. The latter is related to the visual ability to detect a small lesion (12).

$$SNR = \frac{C_{GM} - C_{WM}}{STD_{WM}} \quad (4)$$

$$CNR = \frac{RC}{COV} \quad (5)$$

where C_{GM} and C_{WM} are the GM and WM mean activity concentrations, respectively, and STD_{WM} is the WM STD (background).

2.3. Comparison between reconstruction algorithms

In order to compare the analytical and iterative reconstruction methods available in the workstation at Bralns, PET images were reconstructed with different parameters and algorithms. First, [^{18}F]FDG PET images from the brain simulator were reconstructed as follows:

- i. OSEM (VUE Point HD®, 8 iterations, 16 subsets, 3.0-mm FWHM post-reconstruction smoothing filter, clinical protocol)
- ii. Fourier rebinning (FORE) + filtered back projection (FBP) (enhanced Hanning smoothing filter, 4.8 mm cutoff frequency) and
- iii. FBP (enhanced Hanning smoothing filter)

Standard parameters were used for all reconstruction methods, changing only the acquisition time: 10 min, 5 min, 2.5 min, and 1 min. In this phase, the type of algorithm (analytical or iterative) and acquisition time (1 to 10 min) were evaluated by quantification measurements and image quality parameters.

2.4. Optimization of reconstruction parameters

In this part of the study, [^{18}F]FDG PET images were additionally reconstructed with 4 iterations and 32 subsets. For these settings, we kept the same iterations-subsets product (updates) as the clinical protocol. For the new combination of iterations and subsets, static images were generated for 10 min, 5 min, 2.5 min, and 1 min acquisition times, and different values of the post-smoothing FWHM filter (0 to 10 mm) were used. Quantification measurements and image quality parameters were obtained. Results were compared to the standard reconstruction using the same values of the post-smoothing filter (FWHM varying from 0 to 10 mm).

3. Results and Discussion

3.1. Brain Segmentation

Brain VOIs were automatically created from the CT image using in-house MATLAB® scripts (R2020a, *The MathWorks, Inc.*) by segmenting the GM (270 cm³) and WM (160 cm³) compartments of the brain phantom. The Hoffman brain phantom CT acquisition had a total of 47 slices, from which slices 12 to 28 (center of the phantom) were used to create the masks used in the PET data extraction. Figure 2 shows the GM and WM masks created with our MATLAB® scripts. The results presented in this work were extracted using the eroded versions of these masks.

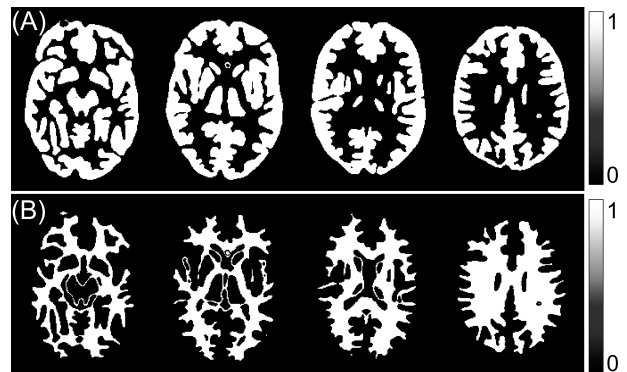


Figure 2. (A) GM and (B) WM masks (binary images) obtained by segmenting the CT image using in-house MATLAB® scripts.

3.1. Comparison between reconstruction algorithms

The reconstruction method OSEM presented the highest SNR (Figure 3A), the lowest quantification bias (Figure 3B) and GM-COV (Figure 3C), when compared to FORE+FBP and FBP for all acquisition times. The COV is less affected by the reconstruction method than by acquisition time. Signal-to-noise ratio and noise estimates for the 5 min reconstructions are similar to those obtained from the 10 min images, with less than 1% difference. SNR results from images reconstructed with OSEM were fairly constant (around 3%) for acquisition times ranging from 2.5 min to 10 min. Quantification bias decreases with the acquisition time, but all three methods presented values lower than 0.7% for 5 min. These results suggest that 5 min would be an adequate choice of acquisition time when compared to the current clinical settings available on this equipment.

3.2. Optimization of reconstruction parameters

Figure 4 shows the result of CNR for the images reconstructed using OSEM with 4 iterations and 32 subsets for a range of post-reconstruction smoothing filter FWHMs (0 = no filter to 10 mm), and acquisition times (1 to 10 min). For comparison, the result from the clinical standard OSEM reconstruction is shown as a point (asterisk), and results for the standard clinical reconstruction for post-reconstruction smoothing filter FWHMs ranging from 0 to 10 mm are shown as a dashed line. The CNR shown in Figure 4 is maximum when the post-reconstruction smoothing filter FWHM ranges from 3

to 6 mm and is comparable to the clinical protocol for all filters (dashed line) for the 5-min acquisition time.

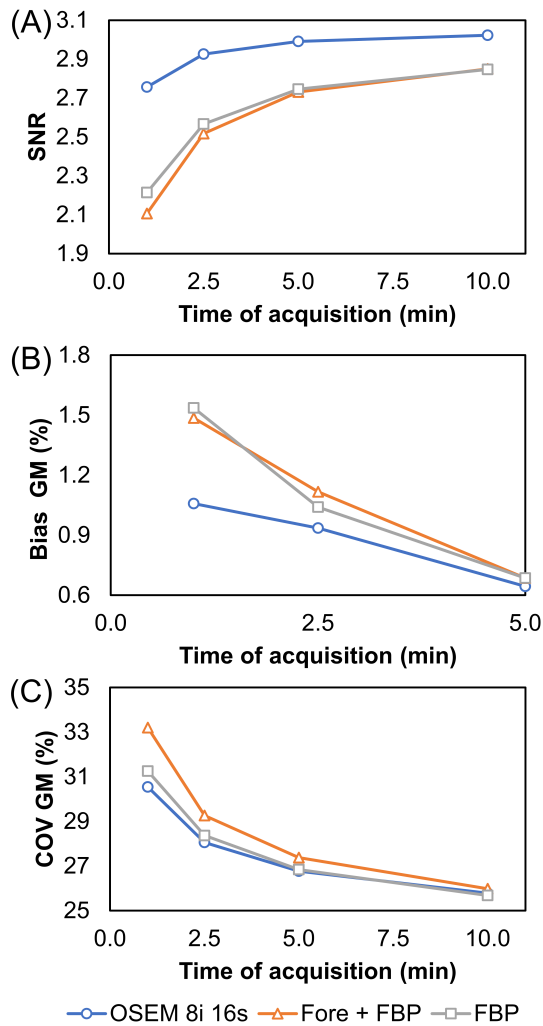


Figure 3. Results of (A) SNR, (B) GM bias (%) and (C) GM-COV (%) measurements for the reconstruction methods (OSEM, FORE+FBP, and FBP), as a function of the acquisition time.

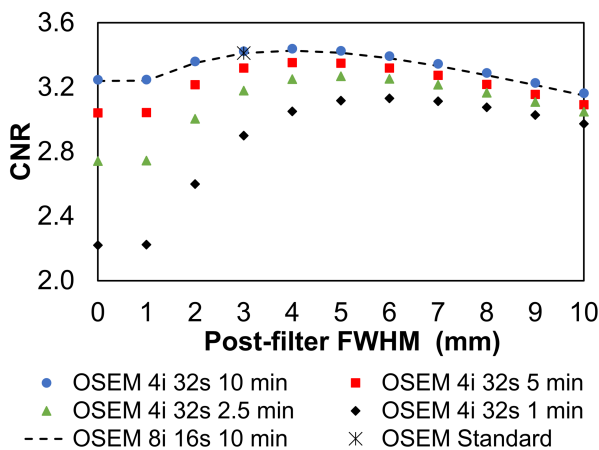


Figure 4. Results of CNR for the OSEM iterative reconstruction method (4 iterations, 32 subsets), plotted as a function of post-reconstruction smoothing filter FWHM. The star point represents the results of the clinical protocol (OSEM, 8 iterations, 16 subsets, 3 mm post-filter FWHM), and the dashed line represent the results of OSEM 8 iterations, 16 subsets 0 to 10 mm post-reconstruction smoothing filter FWHM.

Furthermore, when aiming for a 50% reduction in scan time, images smoothed with a post-reconstruction filter FWHM of 4 mm yielded the maximum CNR results (3.4, approximately 2% less than the current clinical settings). Estimates of RC, GM-COV and SNR were comparable between the 5-min reconstruction (4 mm; 0.877, 26.2%, and 2.97, respectively) and the clinical reconstruction parameters (0.880, 25.8%, and 3.02, respectively). Quantification bias for the OSEM reconstruction method with 4 iterations and 32 subsets was -0.3% when images were reconstructed with 5 min and smoothed with a post-reconstruction filter FWHM of 4 mm.

Moreover, the contrast was comparable between the 5-min reconstruction with post-reconstruction smoothing filter FWHM of 4 mm (2.37) and the clinical reconstruction parameters (2.40). Leemans *et al.* (2015) obtained values of contrast ranging from 2.7 to 3.5, which were directly proportional to the number of iterations when reconstructed using OSEM with 1 to 12 iterations (32 subsets and 45 min acquisition time)²⁶. In a multicenter study (22 PET centres), Habert *et al.* (2016) obtained values of contrast of 3.0 ± 0.3 (range: 2.34 to 3.77; 3×5 min dynamic image) for different equipment and routine iterative reconstruction methods²⁷. The lower contrast obtained in this study was likely due to the shorter image acquisition and differences in equipment and vendor-specific reconstruction algorithms.

A post-reconstruction smoothing filter FWHM of 4 mm was chosen for [¹⁸F]FDG-PET images reconstructed with a 5-min scan based on the results presented here. Such choice was confirmed by the remarkable similarity between the standard clinical protocol (Figure 5A) and images reconstructed with the optimized OSEM parameters (Figure 5B; the percentual difference map is shown in Figure 5C).

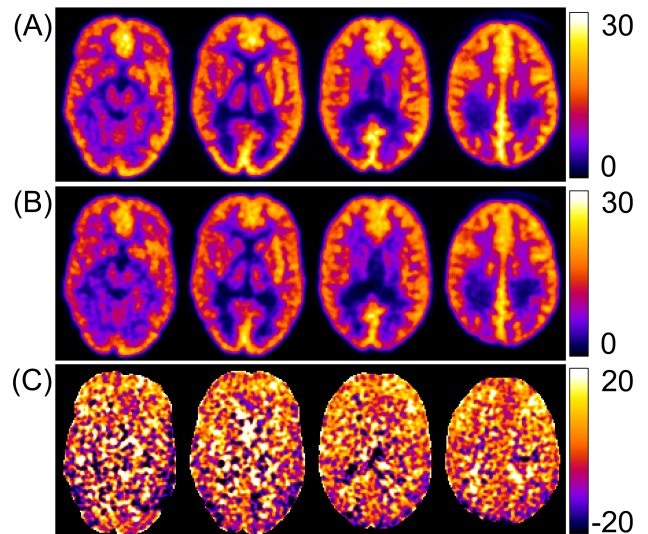


Figure 5. Visual comparison of [¹⁸F]FDG-PET images of the Hoffman 3-D brain simulator reconstructed with (A) the clinical standard (OSEM, 8 iterations, 16 subsets, 3-mm FWHM, 10-min) and (B) the optimized protocol for a 5 min acquisition time (OSEM, 4 iterations, 32 subsets, 4-mm FWHM). The colorbar represents activity concentration (in kBq/mL). Images in line (C) show the percentual difference between (A) and (B).

Previous studies have shown the feasibility of reducing the dose and scanning time in neurological PET imaging studies without affecting diagnostic performance and quantitative assessments (11,26,28–31). In a study with patients with AD and frontotemporal dementia, Schiller *et al.* (2019) suggested the potential to reduce the typical 10 min acquisition time by a factor of 4 without compromising the quality of diagnosis (28). Soret *et al.* (2020) showed that the advantage of dose reduction is a significant decrease in the patient effective dose, which is non-negligible in longitudinal follow-up studies and in research protocols involving healthy volunteers (11). Lastly, Shkumat, Vali and Shammas (2020) showed the feasibility of time (or dose) reduction in the acquisition of [^{18}F]FDG-PET images in studies involving diagnosis, evaluation, and treatment of childhood epilepsy while maintaining the confidence of obtaining diagnostic-quality images (29).

Limitations of this study include the acquisition of [^{18}F]FDG PET/CT data in a single hospital and a limited number of contrast ratios. Further studies, including a variety of equipment and reconstruction settings, and the use of a phantom that allows for a range of contrast ratios, are needed to confirm the results presented here (32). Furthermore, there is a restriction concerning the use a ^{18}F -tracer only, given that the use of higher positron energy radioisotopes would have led to statistical uncertainties due to the random nature of radioactive emissions (33). Additionally, the effect of including a point-spread function correction into the OSEM reconstruction algorithm will be evaluated.

Finally, we are currently investigating the feasibility of reducing the acquisition time by comparing the optimized OSEM parameters with the standard clinical settings. For this, retrospective [^{18}F]FDG-PET data from a clinical study that included individuals with AD will be used (previously approved by the Ethics Committee, CAEA: 00919018.6.0000.5336).

4. Conclusion

Our strategy to analyze the effect of the acquisition time reduction in image quality and quantification metrics in the Hoffman 3-D brain phantom resulted in optimized OSEM reconstruction settings: 4 iterations, 32 subsets and 4 mm post-reconstruction smoothing filter FWHM for a 5 min acquisition time. The 5 min acquisition represents a 50% reduction in imaging time when compared to the standard clinical protocol. With this acquisition time, our results could represent an optimization both in dose costs and radiation protection. The reduction in scan time is significant for patients with neurodegenerative diseases, which results in an increase in patient comfort and limits the image artifacts produced by head movements.

Acknowledgement

This study was financed in part by the Coordenação de Aperfeiçoamento de Pessoal de Nível Superior – Brasil (CAPES) – Finance Code 001 and by CAPES-PRINT-PUCRS.

References

- Saha GB. Basics of PET imaging: physics, chemistry, and regulations. Springer; 2015.
- Cherry S, Sorenson J, Phelps M. Physics in Nuclear Medicine. 2012. 523 p.
- Chauveau F, Boutin H, Van Camp N, Dollé F, Tavitian B. Nuclear imaging of neuroinflammation: a comprehensive review of [^{11}C] PK11195 challengers. *Eur J Nucl Med Mol Imaging*. 2008;35(12):2304–19.
- de Araújo AS, Andrade MA, da Silva AMM. Efeito de Volume Parcial na Quantificação de Imagens PET de Indivíduos Idosos Saudáveis. *Rev Bras Física Médica*. 2018;
- Banati RB, Newcombe J, Gunn RN, Cagnin A, Turkheimer F, Heppner F, et al. The peripheral benzodiazepine binding site in the brain in multiple sclerosis. *Brain [Internet]*. 2000 Nov;123(11):2321–37. Available from: <https://academic.oup.com/brain/article-lookup/doi/10.1093/brain/123.11.2321>
- Jeckel CMM. O uso da Tomografia por Emissão de Pósitrons (pet) no diagnóstico das doenças neurodegenerativas do idoso. *PAJAR - Pan Am J Aging Res*. 2017 Aug;5(1):1.
- Shokouhi S, Riddle W, Kang H. A new data analysis approach for measuring longitudinal changes of metabolism in cognitively normal elderly adults. *Clin Interv Aging*. 2017 Dec;Volume 12:2123–30.
- Prando S, Ono CR, Robilotto CC, Sapienza MT. Methods for quantification of cerebral glycolytic metabolism using 2-deoxy-2- ^{18}F fluoroglucose in small animals. *Res Biomed Eng*. 2018 Sep;34(3):254–72.
- Lim H, Dewaraja YK, Fessler JA. A PET reconstruction formulation that enforces non-negativity in projection space for bias reduction in Y-90 imaging. *Phys Med Biol*. 2018 Feb;63(3):035042.
- Jian Y, Planeta B, Carson RE. Evaluation of bias and variance in low-count OSEM list mode reconstruction. *Phys Med Biol*. 2015 Jan;60(1):15–29.
- Soret M, Piekarski E, Yeni N, Giron A, Maisonneuve J-A, Khalife M, et al. Dose Reduction in Brain [^{18}F]FDG PET/MRI: Give It Half a Chance. *Mol Imaging Biol*. 2020 Jun;22(3):695–702.
- Carrier T, Willowson KP, Fourkal E, Bailey DL, Doss M, Conti M. 90 Y -PET imaging: Exploring limitations and accuracy under conditions of low counts and high random fraction. *Med Phys*. 2015 Jun;42(7):4295–309.
- Yan J, Schaefferkoetter J, Conti M, Townsend D. A method to assess image quality for Low-dose PET: analysis of SNR, CNR, bias and image noise. *Cancer Imaging*. 2016 Dec;16(1):26.
- Grezes-Besset L, Nuyts J, Boellaard R, Buvat I, Michel C, Pierre C, et al. Simulation-based evaluation of NEG-ML iterative reconstruction of low count PET data. In: 2007 IEEE Nuclear Science Symposium Conference Record. IEEE; 2007. p. 3009–14.
- Hamdan AC, Bueno OFA. Relações entre controle executivo e memória episódica verbal no comprometimento cognitivo leve e na demência tipo Alzheimer. *Estud Psicol*. 2005;10(1):63–71.
- Krempser AR, de Oliveira SMV, de Almeida SA. Avaliação do efeito de volume parcial na quantificação de atividade em imagens de PET/CT. *Rev Bras Física Médica*. 2012;6(2):35–40.
- Buvat I. Quantification in emission tomography: Challenges, solutions, and performance. *Nucl Instruments Methods Phys Res Sect A Accel Spectrometers, Detect Assoc Equip [Internet]*. 2007 Feb [cited 2015 Dec 21];571(1–2):10–3. Available from: <http://linkinghub.elsevier.com/retrieve/pii/S0168900206018158>
- Boellaard R. Standards for PET Image Acquisition and Quantitative Data Analysis. *J Nucl Med [Internet]*. 2009 May 1 [cited 2017 Jul 9];50(Suppl_1):11S–20S. Available from: <http://www.ncbi.nlm.nih.gov/pubmed/19380405>
- Tong S, Alessio AM, Kinahan PE. Image reconstruction for PET/CT scanners: past achievements and future challenges. *Imaging Med*. 2010 Oct;2(5):529–45.
- Illes J, Rosen A, Greicius M, Racine E. Prospects for Prediction: Ethics Analysis of Neuroimaging in Alzheimer's Disease. *Ann N Y Acad Sci*. 2007 Feb;1097(1):278–95.
- Wardak M, Wong K-P, Shao W, Dahlbom M, Kepe V, Satyamurthy N, et al. Movement Correction Method for

- Human Brain PET Images: Application to Quantitative Analysis of Dynamic 18F-FDDNP Scans. *J Nucl Med.* 2010 Feb;51(2):210–8.
22. Waxman, A. D., Herholz, K., Lewis, D. H., Herscovitch, P., Minoshima, S., Mountz, J. M., & Consensus GID. Guideline for FDG PET Brain Imaging. 2009.
 23. ICRP. ICRP Publication 106: Radiation Dose to Patients from Radiopharmaceuticals: A third amendment to ICRP Publication 53. 2008.
 24. Dekaban, Anatole S.; Sadowsky D. Changes in brain weights during the span of human life: relation of brain weights to body heights and body weights. *Ann Neurol Off J Am Neurol Assoc Child Neurol Soc.* 1978;4(4):345–56.
 25. Barber TW, Brockway JA, Higgins LS. The density of tissues in and about the head. *Acta Neurol Scand.* 1970 Mar;46(1):85–92.
 26. GE HEALTHCARE. VUE Point HD: Bringing accuracy to PET reconstruction. Waukesha; 2008.
 27. Leemans EL, Kotasidis F, Wissmeyer M, Garibotto V, Zaidi H. Qualitative and Quantitative Evaluation of Blob-Based Time-of-Flight PET Image Reconstruction in Hybrid Brain PET/MR Imaging. *Mol Imaging Biol.* 2015 Oct;17(5):704–13.
 28. Habert M-O, Marie S, Bertin H, Reynal M, Martini J-B, Diallo M, et al. Optimization of brain PET imaging for a multicentric trial: the French CATI experience. *EJNMMI Phys.* 2016 Dec;3(1):6.
 29. Schiller F, Frings L, Thurow J, Meyer PT, Mix M. Limits for Reduction of Acquisition Time and Administered Activity in 18 F-FDG PET Studies of Alzheimer Dementia and Frontotemporal Dementia. *J Nucl Med.* 2019 Dec;60(12):1764–70.
 30. Shkumat NA, Vali R, Shammass A. Clinical evaluation of reconstruction and acquisition time for pediatric 18F-FDG brain PET using digital PET/CT. *Pediatr Radiol.* 2020 Jun;50(7):966–72.
 31. Fällmar D, Lilja J, Kilander L, Danfors T, Lubberink M, Larsson E-M, et al. Validation of true low-dose 18F-FDG PET of the brain. *Am J Nucl Med Mol Imaging.* 2016;6(5):269–76.
 32. Shan ZY, Leiker AJ, Onar-Thomas A, Li Y, Feng T, Reddick WE, et al. Cerebral glucose metabolism on positron emission tomography of children. *Hum Brain Mapp.* 2014 May;35(5):2297–309.
 33. Caribé PRR V., Koole M, D'Asseler Y, Van Den Broeck B, Vandenberghe S. Noise reduction using a Bayesian penalized-likelihood reconstruction algorithm on a time-of-flight PET-CT scanner. *EJNMMI Phys.* 2019 Dec;6(1):22.
 34. Caribé PRR V., Koole M, D'Asseler Y, Deller TW, Van Laere K, Vandenberghe S. NEMA NU 2–2007 performance characteristics of GE Signa integrated PET/MR for different PET isotopes. *EJNMMI Phys.* 2019 Dec;6(1):11.

Contact:

Samara Oliveira Pinto
MEDICOM, PUCRS
Avenida Ipiranga, 6681-Partenon, Porto Alegre, Brasil
CEP 90619-900
samara.pinto@edu.pucrs.br